# Electronic dephasing in nonpolar room temperature liquids: UV photon echo pulse duration dependent measurements

David Zimdars, R. S. Francis, C. Ferrante, and M. D. Fayer[a)]
*Department of Chemistry, Stanford University, Stanford, California 94305*

(Received 26 June 1996; accepted 5 February 1997)

The homogeneous dephasing times, $T_2$, were obtained for the nonpolar chromophore diphenyl acetylene (DPA) dissolved in the room temperature nonpolar solvents 2-methyl pentane (2MP) and cyclohexane. The dephasing times were determined by comparing the pulse duration dependent resonant enhancement of the total two pulse four wave mixing signal to a numerically evaluated theory. Data was taken with 80 and 400 fs transform limited pulses at 300 nm, the electronic origin of DPA in the two solvents. In DPA/2MP, $T_2=120$ fs and in DPA/cyclohexane, $T_2=500$ fs. The analysis required concentration and power dependent measurements to quantitatively determine the resonant enhancement of the signal arising from the addition of DPA to the solvents above the nonresonant solvent only signal. Fundamental experimental difficulties inherent in performing UV femtosecond two pulse photon echoes, in particular the competition with nonresonant signal, are discussed. An efficient numerical algorithm for calculating photon echo decay curves with realistic pulse envelope is described. © *1997 American Institute of Physics.* [S0021-9606(97)00618-1]

## I. INTRODUCTION

Recently, a variety of ultrafast time domain nonlinear optical experiments have been used to directly probe the dynamics of liquid solvent–solute interactions using dye molecules that absorb in the visible or near IR as the probe chromophores. Techniques include the femtosecond photon echo,[1–4] stimulated photon echo,[5,6] and femtosecond hole burning.[7] The experiments show that the dephasing of the electronic transition of the solvated chromophores is dominated by sub-100 fs relaxation processes. The photon echo decays are very rapid, typically the signal decays to less than one percent of the maximum in under 100 fs.[6,8] This has made necessary the use of extremely short optical pulses, less than 20 fs in duration.[1,2] The molecular systems consist of ionic, very polar molecules, e.g., HITCI, in very polar solvents, e.g., ethylene glycol.

Nonpolar molecules in nonpolar liquids at room temperature have not been studied previously with photon echo techniques. Electronic dephasing can be caused by time dependent dipole–dipole interactions between the chromophore and the solvent. The dipoles may be permanent or induced. Ionic dye chromophores and polar solvents have permanent dipole moments. Electronic dephasing of a nonpolar chromophore in nonpolar solvents can only occur through the weaker interactions of induced dipoles. Therefore, nonpolar chromophores are expected to couple less strongly to nonpolar liquids than polar molecules couple to polar liquids, resulting in a relatively slower electronic dephasing.

Molecular dynamics calculations have been performed by Walsh and Loring[9] to simulate the photon echo response for nonpolar chromophores dissolved in a nonpolar solvent. They predict that the echo intensity will fall by one factor of $e$ in 80 to 250 fs at 321 K, depending on the strength of the coupling. A variety of studies indicate that the initial solvent response is a non-Markovian process, while the slower motions are diffusional. This results in a bimodal oscillator-bath time correlation function for dephasing, the short time scale decay is Gaussian followed by a longer time scale exponential component.[8] The analysis is based on the multimode Brownian oscillator model which has been used to describe optical dephasing in liquids.[10,11] For exponential decays (ignoring the initial Gaussian component), the Walsh and Loring calculations for nonpolar systems yield $T_2$'s of 320 to 1 ps.

In this article, the optical dephasing of diphenyl acetylene (DPA), a nonpolar molecule, in two nonpolar liquids, 2-methylpentane (2MP) and cyclohexane will be examined. The origin electronic transition for DPA is at 300 nm, so this article explores the application of UV photon echo experiments to the study of room temperature liquids. In the UV, very strong nonresonant signals fundamentally change the nature of the echo experiment. Because of the strong nonresonant signal, the photon echo decay of DPA could not be well resolved using the standard technique. An alternative method for obtaining the homogeneous dephasing time was developed based on pulse duration dependent experiments. Two sets of two pulse four wave mixing experiments were conducted using 80 and 400 fs transform limited pulses. It is shown that it is possible to obtain the dephasing time by comparing the results of experiments using different pulse durations.

Several topics relevant to performing UV femtosecond photon echo experiments in liquids are discussed below. In a photon echo experiment, two short, intense optical pulses are focused into the sample, crossed at a small angle. The pulses are usually temporally separated so that pulse two interacts in the medium a time $\tau$ after pulse one. The beam geometry satisfies the phase matching conditions $2\mathbf{k}_2-\mathbf{k}_1=\mathbf{k}_s$, where $\mathbf{k}_1$ is the wave vector of the first pulse, $\mathbf{k}_2$ is the wave vector of the second pulse, and $\mathbf{k}_s$ is the wave vector of the gener-

a)Electronic mail: fayer@d31mf0.stanford.edu

 0021-9606/97/106(18)/7498/14/$10.00 

ated signal. The intensity of the signal is recorded as a function of pulse delay $\tau$ yielding a photon echo decay curve. The generated echo pulse shape and delay after the second pulse is usually not resolved, although the signal pulse has been resolved[3,4] by mixing with a short pulse.

This type of short pulse time delayed four-wave mixing experiment will always produce some signal when the pulses are overlapped near zero delay, whether or not the polarization induced in the chromophores are capable of producing a true echo. If the chromophore spectrum is narrow and homogeneous, the ''photon echo'' experiment will produce a decay related to the free induction decay which may be much longer than the pulse duration. If the dephasing time is much shorter than the pulse duration, scanning the delay $\tau$ will generate a curve closely related to the pulse shape and not a decay.[6]

Complicating matters, particularly in the UV, the photon echo signal near $\tau=0$ may not occur solely from resonant interactions with the dissolved chromophores. The nonlinear polarization can be produced nonresonantly by the interaction of the pulses with the solvent. The generic signal obtained will be referred to as ''two pulse four wave mixing'' or ''2PFWM''. The 2PFWM signal can be a mixture of resonant and nonresonant contributions.

For the visible and near IR wavelengths at which most photon echo experiments have been performed, the nonresonant 2PFWM of the pure solvent is far less than the resonant enhancement to the signal by the dissolved chromophores.[1–4] For a given pulse intensity, the resonant contribution to the signal is generally many orders of magnitude greater than the nonresonant contribution. This has permitted the nonresonant signal in 2PFWM experiments to be ignored even though it could, in principle, contribute to a signal in a room temperature liquid.

Working on DPA or other small nonpolar chromophores that absorb in the UV near 300 nm significantly changes the experiment. Although DPA is strongly absorbing, it has a significantly smaller transition dipole moment than visible dye molecules, and it will yield a signal decreased by a factor of $\sim$1000 compared to a dye molecule, other aspects of the experiment being equal. Furthermore, because 300 nm is well within the region for two photon resonance and approaching the one photon resonance of the solvent, the ''nonresonant'' signal is significantly enhanced. As will be shown below, the resonantly enhanced signal near $\tau = 0$ from the dissolved chromophores is buried under the nonresonant 2PFWM signal of the neat solvent.

The experiments and theoretical analysis produce several novel results. Addition of the DPA chromophore to the solvent results in a reduction of the 2PFWM signal, in sharp contrast to experiments in the visible. Absorption of the incident and emitted fields by the chromophores reduces the nonresonant contribution to the signal more than it is enhanced by the resonant contribution. The result is that an echo decay could not be resolved because it is submerged in the nonresonant signal. Nonetheless, a procedure is demonstrated that permits $T_2$ to be obtained for DPA in the two solvents. It is shown that a comparison of the resonant to the nonresonant contribution to the signal that occurs for two durations of transform limited pulses can be used to obtain $T_2$. It is found that $T_2$ is dominated by pure dephasing with $T_2=120$ fs in 2MP and 500 fs in cyclohexane. The theoretical analysis also suggests that using shorter pulses may still make it difficult or impossible to resolve the actual echo decays. While shorter duration pulses will result in a short duration nonresonant contribution to the signal, the magnitude of the nonresonant contribution will grow relative to the resonant contribution. Therefore, the decays will have to be detected further out in time where their magnitude is diminished.

Section II of this article discusses the experimental methods employed. Section III discusses the population dynamics of DPA in 2MP as measured by a single color UV femtosecond pump-probe experiment. Section IV discusses the resonant enhancement of the total nonlinear susceptibility. It is shown that this value depends on the pulse duration. The method for calculating the theoretical 2PFWM signal is discussed. Section V uses the experimental results and numerical calculations of the pulse duration dependent photon echo response to obtain the homogeneous dephasing time for DPA in 2MP and cyclohexane. Appendix A shows the derivation of the affect of linear absorption on pulse duration dependent 2PFWM. Appendix B describes an efficient numerical algorithm for calculating 2PFWM intensity and photon echo decays.

## II. EXPERIMENTAL PROCEDURES

The frequency doubled output of a fiber-prism pulse-compressed amplified femtosecond dye laser system provided UV pulses for the pump-probe and 2PFWM experiments. The fiber and prism pulse compressor were additions to a previously described amplified dye laser system.[12] This system produced pulses at 298 nm, pulse lengths of 80 fs (Gaussian), and energies up to 5 $\mu$J, at a 1 kHz repetition rate. For the pulse duration dependence experiments, the pulse length was increased to a 400 fs transform limited pulse through bypassing the visible fiber which adds bandwidth to the pulse.

While possessing a short central spike, the compressed pulse[13–21] has a broad pedestal.[15,22] By frequency doubling the amplified compressed pulse to perform the UV experiments, the contrast between the pedestal and the central spike was increased to the point where a clean pulse was achieved. Complete details of the laser system are presented elsewhere.[23]

After the pulse compressor, the 600 nm visible pulse is about 30 $\mu$J and 80 fs long. The visible pulse was doubled to 300 nm by focusing to a 500 $\mu$m spot in a 100-$\mu$m-thick type I cut beta–barium borate crystal (BBO). The thin doubling crystal is necessary to double the entire spectral width of a sub 100 fs pulse. It is possible that a slightly shorter pulse could be obtained with a thinner crystal. A conversion efficiency of 10% was achieved, yielding 3 $\mu$J, 300 nm, UV pulses. Up to 10 $\mu$J could be obtained by focusing more tightly at the cost of increasing the pulse length. When the

fiber and compressor are bypassed to double the longer 400 fs pulses, the focus was tightened to compensate for the loss of peak power to achieve similar efficiencies.

A zero order half-wave plate between crossed Glan-laser polarizers was used to adjust the intensity of the UV pulses at the sample. The UV pulse was split into two by a thin 0.125 in. fused silica partially reflecting beam splitter designed for femtosecond autocorrelations. The beam splitter reflected 50% of the light for the photon echo and power/pulse duration dependent four wave mixing experiments. A 10% beam splitter was used for the pump-probe scans. A second 0.125 in. fused silica substrate was placed in the reflected beam at Brewster's angle to ensure both paths had identical material and therefore identical group velocity dispersion (GVD). The probe beam/second pulse traveled down a computer controlled variable optical delay line consisting of a hollow retro reflector (UV aluminum mirrors) mounted on a stepper motor driven translations stage with 0.1 $\mu$m resolution (equivalent to 0.67 fs/step).

The two beams were focused by a 50 cm fused silica lens so that they would overlap noncollinearly at the sample with a diameter ($\pi\omega_0$) of 200 $\mu$m. For the photon echo/2PFWM experiments, the signal is generated coherently in the direction $\mathbf{k}_s=2\mathbf{k}_2-\mathbf{k}_1$. Because of the shorter wavelength, the phase matching condition is more stringent in the UV than in the visible, and the angle between the beams was kept to less than 1°.

The sample path length was 1 mm. The sample was held in a commercial fused silica cuvette in the room temperature pump-probe experiments. In the echo experiments, coherent nonresonant four wave mixing (FWM) signal from the cell windows was made negligible by constructing a special 1 mm path length cell using 200 $\mu$m quartz cover slips as windows.

A reference photodiode sampling the reflection from a quartz flat monitored the intensity fluctuations of the laser. Both the pump-probe and 2PFWM signal were detected by a UV photomultiplier tube placed either in the probe beam or in the phase matched photon echo direction. In the photon echo and FWM experiments, the reference and signal were collected by gated integrators which were optically triggered by the laser. For the pump-probe experiments, a chopper was placed in the pump beam, which blocked every other laser shot. A lock-in amplifier registered the difference in probe signal when the pump was on and off. An A/D converter in a personal computer acquired the signals from the gated integrators or lock-in amplifier. In the FWM experiments, the computer averaged only those data points for which the reference fell within a narrow range of intensity (usually $\pm 10\%$).

The pulses were analyzed for unwanted chirp in the plane of the sample by a modification of the frequency resolved optical grating (FROG) method.[24,25] The UV beams were crossed in the photon echo/2PFWM configuration interior to a piece of quartz mounted inside the sample cell. Because up to 10 $\mu$J of amplified UV energy was available, four wave mixing signal could be generated nonresonantly by the quartz in the $\mathbf{k}_s=2\mathbf{k}_2-\mathbf{k}_1$ direction just as in a resonant photon echo. The signal was spectrally dispersed by a diffraction grating onto a fluorescent card. The temporal overlap of the pulses was then scanned by moving the optical delay line. The signal spectra from a chirped pulse sweeps back and forth as the pulse delay is scanned. The prisms in the pulse compressor were adjusted so that the signal pulse had the full spectrum and no longer swept as the delay line was moved. This corresponded to an unchirped pulse. The pulse duration was then determined by replacing the grating with a detector and recording the nonresonant 2PFWM intensity as a function of pulse delay.

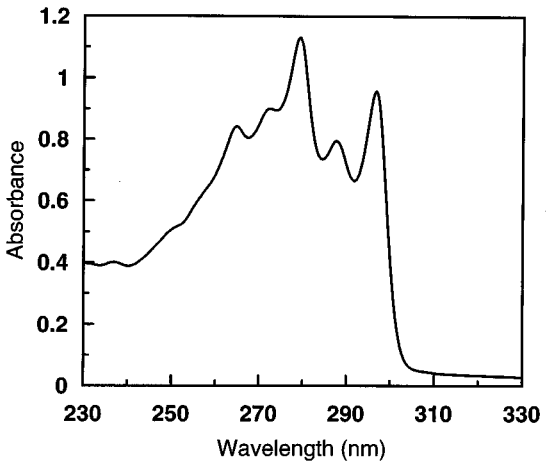


FIG. 1. Absorption spectra of $2.7\times10^{-4}$ M diphenyl acetylene in 2-methyl pentane. The absorbance at the electronic origin of diphenyl acetylene is 0.96 at 297 nm. The molar absorptivity at the origin, $\epsilon$, is about $3\times10^4$ $\ell$/mol cm. The absorbance of the neat solvents is negligible at the experimental wavelength of 298 nm.

Experiments were performed on DPA (Aldrich) in solutions of 2MP (Aldrich), and cyclohexane (Aldrich) without further purification, with the exception of degassing the solvents. Both the pump-probe and 2PFWM experiments were performed at 298 nm, the electronic origin of DPA in these solvents are shown in Fig. 1. The molar absorptivity of DPA at the origin, $\epsilon$, is $\sim3\times10^4$ $\ell$/mol cm. The solvents 2MP and cyclohexane were chosen because they are nonpolar, are not highly polarizable, and have no absorption at 298 nm.

Sample degradation upon moderately short exposure to the intense femtosecond UV pulses was a problem. It was necessary to agitate the liquid to assure that a constant concentration of DPA was present in the beam overlap region. At sufficiently high powers, thermal focusing distorted the 2PFWM signal beyond use.

## III. EXCITED STATE LIFETIME

A pump-probe experiment was performed to measure the ground state recovery lifetime $T_1$ of DPA in 2MP. When analyzing a homogeneous dephasing time, $T_2$, it is necessary to know the lifetime contribution in order to extract the pure dephasing time $T_2^*$. Also, in the calculations performed below, $T_1$ was taken to be much longer than $T_2$. Figure 2 shows the pump probe decay of the electronic origin of $2.7\times10^{-4}$ M DPA in 2MP at 298 K. The apparent change in the absorbance was less than 2%. The solid line through the data is a fit to a single exponential decay plus a baseline

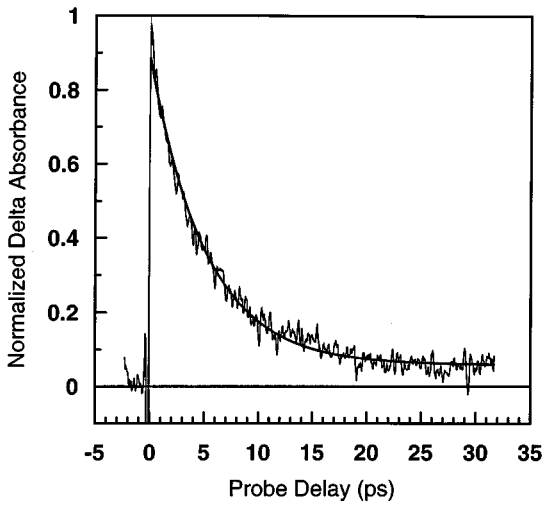


FIG. 2. Pump probe decay of the electronic origin of $2.7\times10^{-4}$ M diphenyl acetylene in 2-methyl pentane liquid at 298 K. The ordinate is probe delay in picoseconds and the abscissa is the change in absorbance normalized to the maximum change. The maximum bleach in the absorbance was less than 2%. The solid line through the data is a fit to a single exponential decay plus an offset. The decay time, $T_1$, is 5.12 ps.

offset. The decay time $T_1$ is 5.12 ps. The offset is due to a long lived triplet state. The pump and probe pulses for this scan had parallel polarizations. Scans were performed at the magic angle (not shown) which indicated that the decay was not affected by rotational diffusion.

These results are in substantial agreement with two-color pump-probe experiments performed by Hirata *et al.*[26] Their decay time for the 500 nm excited state probing was 8 ps.[26] It should be noted that their time resolution was about 4 ps, and their number is the result of a deconvolution.

## IV. THEORY AND METHOD OF PULSE DURATION DEPENDENT 2PFWM DATA ANALYSIS

The change in the resonance enhancement with pulse length was analyzed to obtain values for the homogeneous dephasing time. Although there will be a very short time inertial Gaussian component, the dephasing is treated as exponential characterized by a dephasing time, $T_2$. Given the relatively long dephasing times that are obtained from the experiments, this is not a poor approximation.

While changing the temporal separation between excitation pulses is the norm, changing the duration of the transform limited pulses is another approach to determining $T_2$. This is different than using stretched pulses from a group velocity dispersion delay line as in the experiments by Wiersma *et al.*[27] and our application is substantially different than theirs.

Suppose two different pulse durations, one short and one long, are used to perform a resonant two pulse four wave mixing experiment. For the purposes of this example, the pulses have the same intensity and shape. If the homogeneous dephasing time is much faster than either pulse length, the resultant peak intensities of the signal pulses will be about the same, so that $P(\text{long})/P(\text{short}) \approx 1$ (where here $P$ denotes the peak intensity of the signal pulse). If the dephasing time is much longer than the pulses, the intensity will vary by a constant ratio, dependent on pulse length and dephasing time. The longer pulse will produce a greater ''flip angle'' than the shorter pulse, and the ratio $P(\text{long})/P(\text{short}) \gg 1$. If the dephasing time is somewhere in between, this ratio will decrease. By comparing the experimental value of this ratio to a calculation, $T_2$ can be obtained.

The following is a brief outline of how the quantitative calculation of the dependence of the maximum intensity of the 2PFWM signal on the pulse length and $T_2$ is performed. When the nonlinear polarization for 2PFWM (i.e., photon echo) is calculated using third order diagrammatic perturbation theory,[28,29] the first interaction with pulse 1 and the chromophore can come any time $t_1$ during the envelope of pulse 1. The second and third interactions are with the second pulse and may come any time so long as they follow the strict time ordering $t_3 > t_2 > t_1$. Suppose that in comparison to the pulse durations used in the experiment, the Green function $G_{\text{ba}}(t_2-t_1)$, which determines the dephasing time $T_2$, decays very slowly in time. The strength of the polarization is related to the integral of the pulse envelope (which is determined by the duration of the pulse) times the Green function $G_{\text{ba}}(t_2-t_1)$. In general, if the pulse envelope is longer, the value of this integral will be greater, yielding a more intense echo. So if the pulse duration is varied and $T_2$ held constant, the intensity of the echo will be greater for longer pulse lengths. However, if $T_2$ were to be very short in comparison to the pulse duration, the value of the integral would primarily depend on $T_2$ and not the envelope. Therefore, when $T_2$ becomes fast, two different duration pulses will yield essentially the same photon echo intensities. For a given pair of pulse durations, as $T_2$ becomes longer, for some value of $T_2$, the signal intensities generated by the using the two pulse durations will no longer be the same. This is shown in Fig. 7, which is discussed in Section V.

The experimental signal contains contributions not only from the polarization of the resonant chromophore but from nonresonant polarizations as well. This resonance enhanced signal must be separated from the nonresonant signal. To determine the resonant enhancement, the data must be corrected for the linear absorption and the presence of nonresonant signal. If four wave mixing occurs nonresonantly in a neat solvent, neither the input optical fields nor the generated signal field will be attenuated by linear absorption within the solvent. Suppose, however, that some chromophore is added to the solvent which absorbs linearly (follows Beer's law) but does not contribute to resonant four wave mixing. In this case, the three input fields will be absorbed as they travel to any plane of interaction and the signal field will be absorbed as it travels out of the sample. This attenuation of the nonresonant four wave mixing will be supralinear in the absorber concentration and will dramatically decrease the signal intensity as the concentration of the chromophore is increased. This effect has been partially described before in a different context,[30] but because it is critical to describing how the pulse duration dependent data is analyzed, it has been reformulated in Appendix A. Throughout this article,

the effect of linear absorption will be termed the ''inner filter'' since it is a result of the propagation of the optical field inside the sample. Since the chromophore does resonantly generate a four wave mixing signal, this signal will be attenuated as well by the inner filter effect.

Like degenerate four wave mixing (DFWM), the photon echo satisfies the frequency matching conditions $\omega_s = \omega 3 + \omega_2 - \omega_1$ with $\omega = \omega_s = \omega_3 = \omega_2 = \omega_1$. For the photon echo, the optical field $\omega_1$ comes from the first pulse and the optical fields $\omega_2$ and $\omega_3$ come from the second pulse. If the pulse shapes and temporal overlap of the pulses are kept constant, and possible dispersive effects which affect the phase of the generated ''echo'' pulse are omitted, the response to a pulse of arbitrary maximum electric field at a given central frequency can be calculated by integrating the time domain dependences. This response will be denoted as a modified susceptibility $\hat{\chi}^{(3)}(\omega;\tau_p)$, where the overscore serves as a reminder that temporal dependences not present in the ordinary form may be hidden in the expression. Since this susceptibility is specifically for a degenerate four wave mixing process, only one of the four frequencies associated with a general expression of the third order nonlinear susceptibility is explicitly written. This susceptibility is defined to be used with three electric field plane waves of the form $E = E_0 \xi(t;\tau_p)\exp(\pm i\omega t)$ each with the same frequency $\omega$ and identical pulse envelopes $\xi(t,\tau_p)$. The parameter $\tau_p$ denotes the pulse duration. Note that each susceptibility $\hat{\chi}^{(3)}(\omega;\tau_p)$ is defined for only one functional form of the envelope $\xi(t,\tau_p)$ at one pulse duration $\tau_p$. Once the envelope is assumed, the electric fields will be denoted only by the complex amplitude of each electric field (this amplitude need not be identical for each field). The possibility of detecting a pulse duration dependence in the resonant susceptibility is the key to obtaining a dephasing time from the two pulse four wave mixing data if there is no proper photon echo decay or if the signal is too weak to detect the decay.

The third order nonlinear polarization is then:

$$P^{(3)}(\omega) = \hat{\chi}^{(3)}(\omega;\tau_p) E_1^* E_2^2. \tag{4.1}$$

Note once again that the quantities ''$E$'' are the complex amplitudes for the specific electric fields with pulse duration and envelope function not explicitly written. The resultant polarization $P^{(3)}_{\rm tot}(\omega)$ also has an unstated envelope. For the purpose of summing polarizations from different sources, it will be assumed that this envelope can be well approximated by a step function with duration $\tau_p$ and amplitude given by Eq. (4.1).

The total third order nonlinear susceptibility, $\hat{\chi}^{(3)}_{\rm tot}$, is written as the sum of resonant, $\hat{\chi}^{(3)}_r$, and nonresonant, $\hat{\chi}^{(3)}_{\rm nr}$, portions:

$$\hat{\chi}^{(3)}_{\rm tot}(\omega,\tau_p) = \hat{\chi}^{(3)}_r(\omega;\text{chromophore, concentration},\tau_p) + \hat{\chi}^{(3)}_{\rm nr}(\omega;\text{solvent},\tau_p). \tag{4.2}$$

Both terms have a frequency dependence $\omega$. The nonresonant frequency dependence of $\hat{\chi}^{(3)}_{\rm nr}$ is due to properties intrinsic to the solvent. Note that the nonresonant susceptibility may have a pulse duration dependence. While a portion of the four wave mixing processes responsible for the nonresonant susceptibility involves virtual states which dephase instantaneously, it is necessary to account for the formation of a nuclear Kerr grating in the liquid, which does not dissipate instantaneously. The resonant frequency dependence of $\hat{\chi}^{(3)}_r$ is due to properties of the chromophore such as the transition dipole moment and the concentration of chromophore in the solvent.

The intensity of an optical pulse is related to the electric field by $I \propto |E|^2$. In practice, it is easiest to vary the energy, or time integrated intensity of the pulse. The energy of the pulse will be denoted as $U$. The detected signal energy is denoted $U_s$. For simplicity, the pulses are taken to be square, which does not change the nature of the results. This has been tested using Gaussian envelopes.

$$U = \int E^2 dt \approx E^2 \tau_p, U_s = \int |P^{(3)}|^2 dt \approx (P^{(3)})^{(2)} \tau_p. \tag{4.3}$$

The pulse duration $\tau_p$ occurs here to properly normalize the amplitude of the electric fields.

When the resonant susceptibility is present, the signal energy must be corrected for linear absorbance (inner filter). Since the nonresonant signal in a pure solvent sample suffers from no absorbance, no correction is necessary. Appendix A describes the derivation of the inner filter correction factor $f^{(3)}(A)$ as a function of Beer's law absorbance. The ratio of the energy of the resonant plus nonresonant signal divided by the nonresonant signal alone [Eqs. (A8) and (A9) in Appendix A, respectively] gives:

$$\frac{U_{\rm tot}}{U_{\rm nr}} = \frac{\beta_{\rm tot}}{\beta_{\rm nr}} \frac{|\hat{\chi}^{(3)}_{\rm tot}|^2}{|\hat{\chi}^{(3)}_{\rm nr}|^2} f^{(3)}(A). \tag{4.4}$$

The factor $\beta$ corrects for the slight change in pulse shape of the signal from resonant to nonresonant. The ratio of $U_{\rm tot}/U_{\rm nr}$ and the absorbance A can be determined experimentally. Note that the ratio in Eq. (4.4) does not contain any dependence on the input pulse energy $U_0$ or the pulse duration $\tau_p$ and that the expression has no dependence on the sample length $l$ [as in Eqs. (A8) and (A9) in Appendix A] except as contained in the absorbance A. The total susceptibility still contains a possible resonant susceptibility dependence on the pulse duration, $\tau_p$. Since the pulse shape coefficients $\beta$ are nearly the same, the expression of Eq. (4.4) for intensity and energy are essentially the same.

The inner filter function for the third order polarization is (Appendix A):

$$f^{(3)}(A) = \frac{10^{-A}[10^{-A}-1]^2}{(\ln 10)^2 A^2}. \tag{4.5}$$

This third order inner filter function $f^{(3)}(A)$ is plotted versus absorbance A in Fig. 3.

It is necessary to determine if an observed ratio of $U_{\rm tot}/U_{\rm nr}$ is indicative of a resonant enhancement by a chromophore of concentration $c$ in solution. Rearranging Eq. (4.4) and writing $\hat{\chi}^{(3)}_{\rm tot}$ as defined by Eq. (4.1) yields:

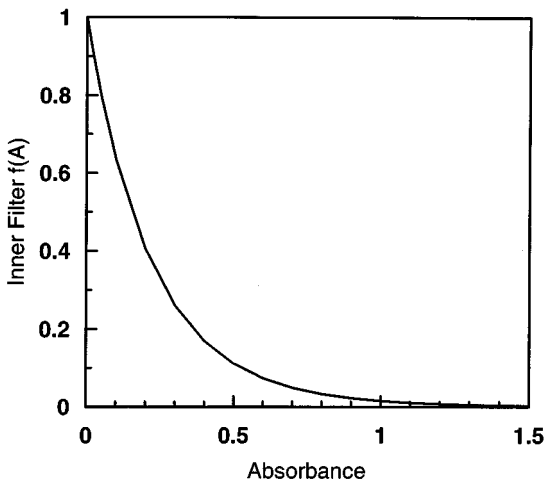


FIG. 3. Plot of $f^{(3)}(A)$ vs the absorbance $A$: $f^{(3)}(A)$ is the attenuation of a resonant four wave mixing signal due to the linear absorbance $A$ of the sample.

$$\frac{|\hat{\chi}_r^{(3)}(\tau_p,c)+\hat{\chi}_{\rm nr}^{(3)}|^2}{|\chi_{\rm nr}^{(3)}|^2}=\frac{U_{\rm tot}}{U_{\rm nr}}[f^{(3)}(\mathrm{A})]^{-1}. \tag{4.6}$$

The experimental ratio of $U_{\rm tot}/U_{\rm nr}$ multiplied by the ''inverse inner filter'' equals the ratio of the susceptibilities. If this ratio is greater than one, then the chromophore is participating in a resonant enhancement of the signal.

Equation (4.6) from can be manipulated to determine the ratio of the resonant to nonresonant susceptibilities. $\hat{\chi}_r^{(3)}\propto c$, where $c$ is the concentration of the resonant chromophore. If it is assumed that the contributions of the resonant and nonresonant susceptibilities are substantially in phase, then

$$\left|\frac{\hat{\chi}_r^{(3)}}{\hat{\chi}_{\rm nr}^{(3)}}\right|^2 c^2=\left[\left(\frac{U_{\rm tot}}{U_{\rm nr}}[f^{(3)}(A)]^{-1}\right)^{1/2}-1\right]^2. \tag{4.7}$$

The factor $|\hat{\chi}_r^{(3)}/\hat{\chi}_{\rm nr}^{(3)}|^2$ can be determined by using the experimental data $U_{\rm tot}/U_{\rm nr}$ and the absorbance $A$ to fit the right hand side of Eq. (4.7) to a quadratic concentration dependence.

The details of the calculations that yield $T_2$ from the pulse duration dependence of the energy from a purely resonant signal are presented in appendices. In the notation of Eq. (A8), but without the inner filter correction, the energy of the resonant signal is:

$$U_r(\tau_p;T_2)=|\hat{\chi}_r^{(3)}|\,\frac{U_0^3}{\tau_p^2}. \tag{4.8}$$

The ratio of the signal energy from the nonresonant contribution $U_{\rm nr}(\tau_l)/U_{\rm nr}(\tau_s)$ for two different pulse durations denoted ''$\tau_l$'' for long and ''$\tau_s$'' for short can be measured, and the ratio of the purely resonant signal energy $U_r(\tau_l)/U_r(\tau_s)$ for the same pulse durations can be calculated by the method described below.

These two quantities can be combined as follows and expanded using Eq. (A9) and Eq. (4.8):

$$\frac{U_r(\tau_l)}{U_r(\tau_s)}\,\frac{U_{\rm nr}(\tau_s)}{U_{\rm nr}(\tau_l)}=\left[\frac{|\hat{\chi}_r^{(3)}(\tau_l)|^2U_0^3/\tau_1^2}{|\hat{\chi}_r^{(3)}(\tau_s)|^2U_0^3/\tau_s^2}\right]\times\left[\frac{|\hat{\chi}_{\rm nr}^{(3)}(\tau_s)|^2U_0^3l^2/\tau_s^2}{|\hat{\chi}_{\rm nr}^{(3)}(\tau_l)|^2U_0^3l^2/\tau_1^2}\right]. \tag{4.9}$$

Equation (4.9) can be rearranged (the energy and pulse durations cancel) to give an expression that contains only calculable and measurable quantities:

$$\frac{U_r(\tau_l)}{U_r(\tau_s)}=\left[\frac{U_{\rm nr}(\tau_l)}{U_{\rm nr}(\tau_s)}\right]\left[\left|\frac{\hat{\chi}_r^{(3)}(\tau_l)}{\hat{\chi}_{\rm nr}^{(3)}(\tau_l)}\right|^2\right]\left[\left|\frac{\hat{\chi}_r^{(3)}(\tau_s)}{\hat{\chi}_{\rm nr}^{(3)}(\tau_s)}\right|^2\right]^{-1}. \tag{4.10}$$

With the known pulse durations as inputs, the calculated ratio of the resonant signal energies on the left-hand side of Eq. (4.10) will be fit (Sec. V) as a function of $T_2$ to the product of the three experimental quantities on the right-hand side of Eq. (4.10). These values are given by the fits to Eq. (4.7) and the experimental value of the ratio of the nonresonant energies.

For brevity's sake, the measured ratio given by Eq. (4.7) $|\hat{\chi}_r^{(3)}(\tau_p)/\hat{\chi}_{\rm nr}^{(3)}(\tau_p)|^2$ for pulse duration $\tau_p$ will be denoted as $R_{r/\rm nr}(\tau_p)$. The measured ratio $U_{\rm nr}(\tau_l)/U_{\rm nr}(\tau_s)$ will be denoted as $R_{\rm nr}(\tau_l,\tau_s)$. Thus the right-hand side of Eq. (4.10) would be denoted as $R_{\rm nr}(\tau_l,\tau_s)R_{r/\rm nr}(\tau_l)/R_{r/\rm nr}(\tau_s)$.

To fit data to Eq. (4.10), the signal energy of a purely resonant 2PFWM signal must be calculated. Since the experiments are concerned with the dependence of the signal $U_r(\tau_p;T_2)$ on the pulse duration $\tau_p$, the theory and calculations will be presented in the time domain, unlike the derivation of Eq. (4.10). The details of the method are presented in Appendix B.

Third order diagrammatic perturbation theory was used to calculate the resonant nonlinear polarization $P^{(3)}(t_s,\tau)$ for all contributions to the signal at wave vector $2\mathbf{k}_2-\mathbf{k}_1$. Here $t_s$ is time for the polarization and $\tau$ is the separation between pulses. The method solves the equation of motion in Louiville space perturbatively for the initial density matrix and three interactions with an optical field.[28,29] The trace of the density matrix with the dipole moment operator gives the resulting nonlinear polarization. Double sided Feynman diagrams can be drawn which depict the pathway through Liouville space for each possible time and frequency ordering of the electric fields which meet the experimental conditions. The electronic transition is modeled as a two level system with ground state $|a\rangle$ and excited state $|b\rangle$. There are four double sided Feynman diagrams which contribute signal in the $\mathbf{k}_s=2\mathbf{k}_2-\mathbf{k}_1$ direction.[28,29] Two of these diagrams have interactions which correspond with the time ordering of the applied pulse sequence and are responsible for the photon echo. The other two diagrams have interactions which do not correspond to the ordering of the pulse sequence. These diagrams only contribute to a nonzero $P^{(3)}$ when the delay is short enough that the electric field envelopes overlap.

The expression for $P^{(3)}$ can be written from these diagrams directly by using the methods described in Refs. 30 and 31. $P^{(3)}$ can be obtained in closed form for only a few temporal pulse shapes given by $\xi_{\mathbf{k}_1}(t')$ and forms of the

Liouville propagators $G_{ij}(t''-t')$. In general, these solutions of $P^{(3)}$ require the fields to be cw or completely impulsive [$\xi_{\mathbf{k}_1}(t')$ is constant or a delta function]. Realistic Gaussian or hyperbolic secant squared shaped envelopes require numerical evaluation. $P^{(3)}$ is obtained in Appendix B. The functional form of the Liouville propagators $G_{ij}(t''-t')$ are determined by the model of the material system. As discussed in detail in Appendix B, the simplest form of the propagator was selected such that homogeneous dephasing is described in terms of $T_2$ where $T_2$ is the same as in the Bloch picture.

The expression above for $P^{(3)}$ is at a minimum a three-dimensional integral. To calculate the observable, $P^{(3)}$ must be integrated over the inhomogeneous line and then the modulus square of the result must be integrated over all time. The expression for the signal energy of a photon echo is:

$$U_s[\tau,\xi(\tau_p),T_2] \propto \int_{-\infty}^{\infty} dt_s \left| \int_0^{\infty} d\omega_{\mathrm{ba}} g(\omega_{\mathrm{ba}}) P^{(3)}_{\mathrm{total}}[t_s,\omega_{\mathrm{ba}},\tau,\xi(\tau_p),T_2] \right|^2, \tag{4.11}$$

where $g(\omega_{\mathrm{ba}})$ is the inhomogeneous distribution and $\tau$ is the separation between the two laser pulses. The homogeneous dephasing time $T_2$ is shown as an explicit parameter in Eq. (4.11) as reminder that the model for the polarization damping has been chosen, and, more importantly, that $T_2$ will be the fitting parameter in Eq. (4.12). Equation (4.11) illustrates that any numerical simulation of the photon echo decay with realistic laser pulse envelopes and realistic material damping will involve a five dimensional integral.

By comparison to Eq. (4.10) and using the abbreviated notation for the right-hand side, if Eq. (4.11) is evaluated for two pulses of different durations, one long ($\tau_1$) and one short ($\tau_s$) then:

$$\frac{U_s(\xi(\tau_1),T_2)}{U_s(\xi(\tau_s),T_2)} = R_{\mathrm{nr}}(\tau_1,\tau_s) R_{r/\mathrm{nr}}(\tau_1)/R_{r/\mathrm{nr}}(\tau_s), \tag{4.12}$$

where all parameter except for the pulse duration have been kept the same. This ratio can be calculated for a series of homogeneous dephasing times $T_2$ and compared to the experimental value of the ratio. The left-hand side of Eq. (4.12) can be determined by calculating Eq. (4.11) using the experimental values, except for $T_2$, which is the free parameter. As mentioned above, evaluation of Eq. (4.11) for use in Eq. (4.12) requires numerical integration. Appendix B discusses the method used to efficiently calculate these values for use in fitting the data in Sec. V.

## V. EXPERIMENTAL RESULTS

### A. UV 2PFWM corrected for linear absorbance

Time resolved two pulse four wave mixing scans were taken on samples of DPA dissolved in 2MP liquid at room temperature. Within the signal to noise, there was no deviation from the shape of the trace generated in the pure solvent or in a quartz slide. The scans taken on the DPA solution had worse signal to noise than from pure 2MP because the total four wave mixing signal decreased by up to a factor of 10, depending on the DPA concentration. The resonance enhancement of the nonlinear susceptibility did not overcome the attenuation effects of linear absorption. This does not imply that the data were totally nonresonant, but without a detailed correction for linear absorption, it is not possible to say what fraction of the signal arises from resonant interactions.

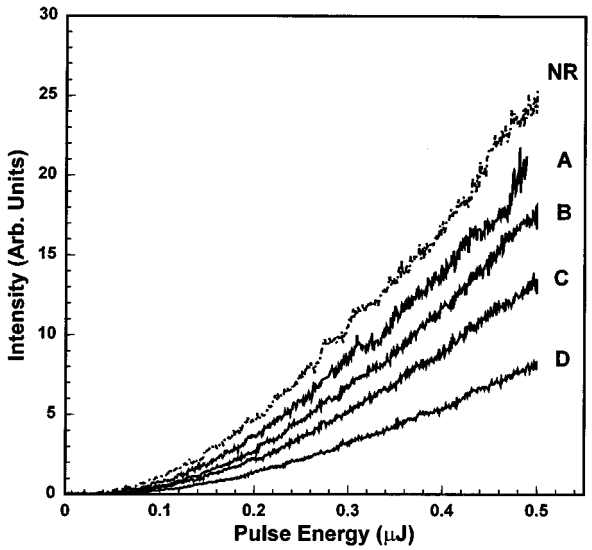


FIG. 4. Ultraviolet two pulse four wave mixing signal detected in the $\mathbf{k}_s = 2\mathbf{k}_2 - \mathbf{k}_1$ direction vs pulse energy for 400 fs, 298 nm pulses of diphenyl acetylene (DPA) in cyclohexane. This data have not been corrected for linear absorbance. NR: Nonresonant two pulse four wave mixing signal of cyclohexane (no absorbance). A: DPA absorbance=0.16.; B: DPA absorbance=0.32; C: DPA absorbance=0.63; D: DPA absorbance=1.19. The intensity of the total two pulse four wave mixing signal (resonant and nonresonant) decreases monotonically with increasing DPA concentration. Although the optical pulses are resonant with the electronic origin of diphenyl acetylene, the resonant nonlinear susceptibility is not large enough to overcome the linear absorption of the chromophore.

The resonant enhancement of the nonlinear susceptibility was quantitatively determined by fitting concentration dependent two pulse four wave mixing data. The intensity of the nonlinear signal versus input pulse intensity at each concentration was corrected for linear absorbance. The power dependences are normalized by the nonresonant power dependence of the neat solvent to correct for the pulse length and intensity dependence. The data were fit to a quadratic concentration dependence to yield the resonant enhancement for the chromophore for the particular pulse length used. The experiments were performed at two pulse durations, which allowed the homogeneous dephasing time to be obtained.

The UV two pulse four wave mixing signal detected from DPA in cyclohexane versus pulse energy for 400 fs, 298 nm pulses is shown in Fig. 4. This data has not been corrected for linear absorbance. Note that the intensity of the total two pulse four wave mixing signal (resonant and nonresonant) decreases monotonically with concentration. Although the optical pulses are resonant with the electronic origin of DPA, the resonant nonlinear susceptibility is not

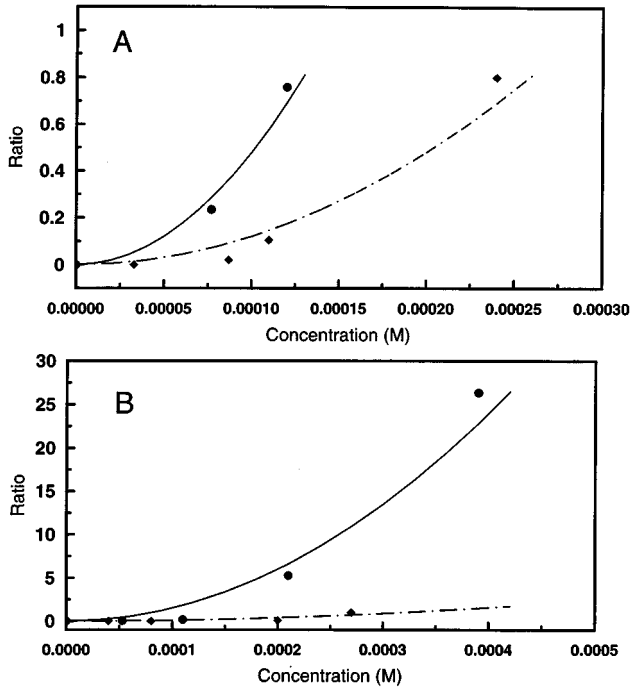


FIG. 5. (a) Ratios of resonant plus nonresonant signal to the nonresonant signal for diphenyl acetylene in 2-methyl pentane vs the concentration of diphenyl acetylene. Diamonds: 80 fs pulse length. Broken line: Fit. Circles: 400 fs pulse length. Solid line: Fit. Values are corrected for linear absorbance. (b) Ratios of resonant plus nonresonant signal to the nonresonant signal for diphenyl acetylene in cyclohexane vs the concentration of diphenyl acetylene. Diamonds: 80 fs pulse length. Broken line: Fit. Circles: 400 fs pulse length. Solid line: Fit. Values are corrected for linear absorbance.

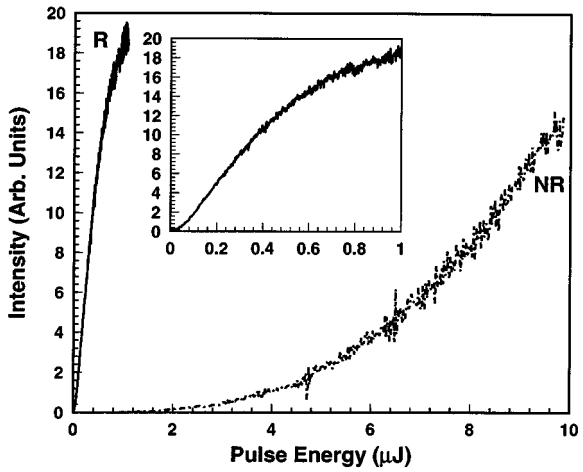


FIG. 6. Visible two pulses four wave mixing signal detected in the $\mathbf{k}_s=2\mathbf{k}_2-\mathbf{k}_1$ direction vs pulse energy for 400 fs, 600 nm pulses of cresyl violet (CV) in deuterated ethanol (EtOD). This data has not been corrected for linear absorbance. NR: Nonresonant two pulse four wave mixing signal of EtOD (no absorbance). R: Resonant plus nonresonant two pulse four wave mixing signal of CV, absorbance $A=0.8$. For this visible dye, the resonant signal overwhelms the nonresonant signal. Inset: The resonant plus nonresonant curve plotted with an expanded ordinate. The resonantly enhanced signal deviates from a cubic power dependence above 300 nJ.

large enough to overcome the linear absorption of the chromophore.

The values of Eq. (4.7), given by the ratios of resonant plus nonresonant signal to the nonresonant signal for DPA in 2MP versus the concentration of DPA are shown in Fig. 5(a). The diamonds show the data for 80 fs pulses, and the broken line is the best fit to a concentration dependence of $R_{r/\mathrm{nr}}(80)[c]^2$ with $R_{r/\mathrm{nr}}(80)=1.2\times10^7\ \mathrm{M}^{-2}$. The circles show the data for 400 fs pulses, and the solid line is the best fit to a concentration dependence of $R_{r/\mathrm{nr}}(400)[c]^2$ with $R_{r/\mathrm{nr}}(400)=4.8\times10^8\ \mathrm{M}^{-2}$. The resonant two pulse four wave mixing intensity has been corrected for the linear absorbance of the solute using Eq (4.6). Increasing the pulse length by a factor of 5 gives a ratio of $R_{r/\mathrm{nr}}(400)/R_{r/\mathrm{nr}}(80)=4.0$. The ratio of the nonresonant signal energies for the two pulse lengths $R_{nr}(40\,080)$ was 0.51. The fact that this number was not substantially smaller indicates that a portion of the nonresonant signal arises from a nuclear Kerr effect grating in the liquid. The calculated ratio of the resonant energies that matches the experimental value of $R_{\mathrm{nr}}(40\,080)R_{r/\mathrm{nr}}(400)/R_{r/\mathrm{nr}}(80)=2.04$ will yield $T_2$ for DPA in 2MP.

The values of Eq. (4.7) given by the ratios of resonant plus nonresonant signal to nonresonant signal for DPA in cyclohexane versus the concentration of DPA are shown in Fig. 5(b). The diamonds show the data for 80 fs pulses, and the broken line is the best fit to a concentration dependence of $R_{r/\mathrm{nr}}(80)[c]^2$ with $R_{r/\mathrm{nr}}(80)=1\times10^7\ \mathrm{M}^{-2}$. The circles show data for 400 fs pulses, and the solid line is the best fit to a concentration dependence of $R_{r/\mathrm{nr}}(400)[c]^2$ with $R_{r/\mathrm{nr}}(400)=1.5\times10^8\ \mathrm{M}^{-2}$. The resonant two pulse four wave mixing intensity has been corrected for the linear absorbance of the solute. Increasing the pulse length by a factor of 5 gives a ratio of $R_{r/\mathrm{nr}}(400)/R_{r/\mathrm{nr}}(80)=15$. The ratio of the nonresonant signal energies for the two pulse lengths $R_{\mathrm{nr}}(40\,080)$ was 0.63. The calculated ratio of the resonant energies that matches the experimental value $R_{\mathrm{nr}}(40\,080)R_{r/\mathrm{nr}}(400)/R_{r/\mathrm{nr}}(80)=6.45$ will yield $T_2$ for DPA in cyclohexane.

For both cyclohexane and 2-methyl pentane, the data show the expected quadratic dependence on concentration. Also, the data show that the two pulse four wave mixing is more intense for longer pulses of the same energy. This implies that $T_2$ is greater than or about equal to the pulse length.

Both solutions of DPA show a resonance enhancement with the addition of the chromophore. However, in comparison with typical visible laser dyes, this enhancement is small relative to the nonresonant contribution. For comparison, Fig. 6 shows the visible two pulses four wave mixing signal detected in the $\mathbf{k}_s=2\mathbf{k}_2-\mathbf{k}_1$ direction versus pulse energy for 400 fs, 600 nm pulses on a sample of $3\times10^{-4}$ mol/ cresyl violet (CV) in deuterated ethanol. The sample path length was 1.0 mm, and the spot size is 200 $\mu$m. This data has not been corrected for linear absorbance, and as can be seen, no correction is necessary in order to determine that a substantial resonant enhancement exists for CV. The resonant signal is very large for pulse energies that give essentially zero nonresonant signal. The inset shows the two pulse four wave

mixing of CV, plotted with an expanded ordinate. The resonantly enhanced signal deviates from a cubic power dependency above 300 nJ indicating that the third order nonlinear process is no longer in the low power limit.

The total two pulse four wave mixing of the chromophore cresyl violet shows a large resonant enhancement in comparison to diphenyl acetylene at 298 nm. At this concentration, CV exhibits what is expected of a dye in the visible–monotonically increasing signal with addition of chromophore. The resonantly enhanced signal (in the cubic regime) is approximately 3000 times that of the nonresonant signal alone without any correction for linear absorbance. When corrected for the linear absorbance $A$ of 0.8, the observed signal is reduced by a factor of 0.033. Thus the ratio $|\chi^{(3)}_{\mathrm{tot}}|^2/|\chi^{(3)}_{\mathrm{nr}}|^2$ for CV in the visible at 600 nm is about 86 000. This is in contrast to the situation in the UV where the ratio for DPA with the same absorbance is about 4. This demonstrates an inherent difficulty in conducting ultrafast photon echo experiments in liquids on molecules that absorb in the UV.

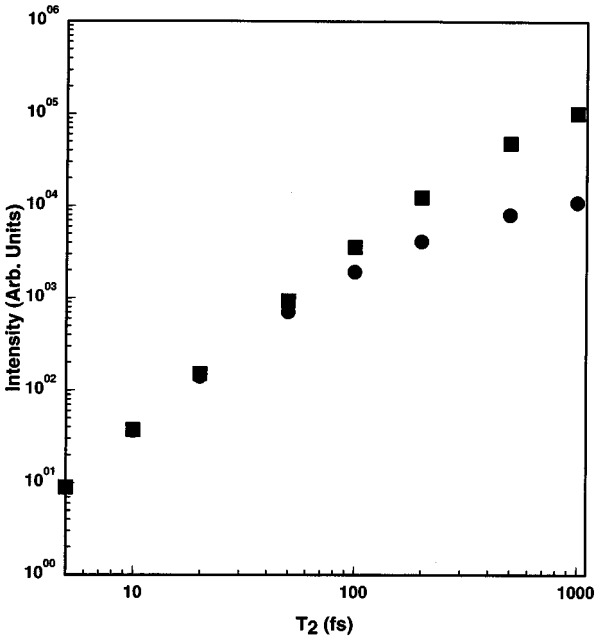


FIG. 7. Logarithmic plot of the calculated maximum energy of the 2PFWM signal vs the phenomenological dephasing time $T_2$ for DPA in a solvent. Circles: pulse 1 and 2, 80 fs. Squares: pulse 1 and 2, 400 fs. The calculations were performed using realistic optical pulses with Gaussian electric field envelopes. The calculations were made corresponding to the pulse lengths and parameters of the room temperature resonant two pulse four wave mixing experiments. While having differing pulse lengths, the pulses have identical energies. As $T_2$ becomes longer, the difference in the signal intensity increases. Therefore, the ratio of the signal intensities for two transform limited pulse durations can be used to obtain $T_2$.

### B. Determination of $T_2$

As discussed in Sec. IV, it is possible to determine the homogeneous dephasing time, $T_2$, by comparing the right-hand side of Eq. (4.12) determined above from the experiments to the left-hand side obtained from theoretical calculations of the 2PFWM signal $U_s$ as a function of the free parameter $T_2$. Equation (4.11) expresses the signal energy. In the calculation of $U_s$ for use in Eq. (4.12), the other parameters (in particular the pulse duration $\tau_p$) are fixed by experimental conditions.

The calculations were performed using realistic optical pulses with Gaussian electric field envelopes. Gaussian pules were used since they best matched the frequency doubled pulses used in the experiments. While having differing pulse lengths, the pulses had identical energies. The pulse separation $\tau$ was not zero but corresponds to the delay where the 2PFWM signal was maximum. These were the conditions used in the experiments. Appendix B describes the numeric integration of Eq. (4.11) in detail.

Calculations were made to determine the relative strength of the 2PFWM experiments as measured by the concentration and power dependences described above. Figure 7 shows a logarithmic plot of the calculated maximum energy of the two pulse photon echo signal [Eq. (4.11)] versus the phenomenological dephasing time $T_2$. The optical pulse frequency was $1.01\times10^{15}$ Hz (wavelength=298 nm), the inhomogeneous line center frequency was $1.01\times10^{15}$ Hz (wavelength=298 nm), and the full width at half maximum (FWHM) of the inhomogeneous line was $3\times10^{14}$ Hz.

Two sets of calculations were made corresponding to the pulse lengths and parameters of the room temperature resonant two pulse four wave mixing experiments. The circles show the values for 80 fs FWHM Gaussian pulses. The squares show the values for 400 fs FWHM Gaussian pulses. Note that as expected, when $T_2$ is on the order of the pulse length, the peak intensity as a function of pulse length begins to depend on $T_2$. At $T_2=50$ fs, the longer pulse is beginning to produce a greater signal intensity. For $T_2=200$ fs, there is a substantial difference, and by $T_2=500$ fs, the difference is almost an order of magnitude.

The ratio of the maximum intensity of the two pulse photon echo decay for 400 fs Gaussian pulses to that of 80 fs Gaussian pulses versus the phenomenological dephasing time $T_2$ is shown in Fig. 8. This curve is the ratio of the two curves in Fig. 7 and the parameters for the calculation are the same. These values correspond to the ratio on the left-handside of Eq. (4.12). Because this ratio is smooth, monotonically increasing function, it can be used to evaluate $T_2$ for the experimental data. Experimental results for DPA in the two solvents were used to obtain numbers for the right-handside of Eq. (4.12) in Sec. V A.

The open circle is the experimental ratio of 2.04 found for DPA in room temperature 2-methyl pentane and corresponds to a dephasing time, $T_2=120$ fs. The hatched circle is the experimental ratio of 6.45 found for DPA in room temperature cyclohexane and corresponds to a dephasing time, $T_2=500$ fs. These correspond to exponential photon echo decay constants of 30 and 125 fs, respectively. An estimate of the propagation of experimental error makes the maximum uncertainty $\sim$25%.

The $T_2$'s were obtained without using the normal scanning of the delay. An important question, which can be ad-

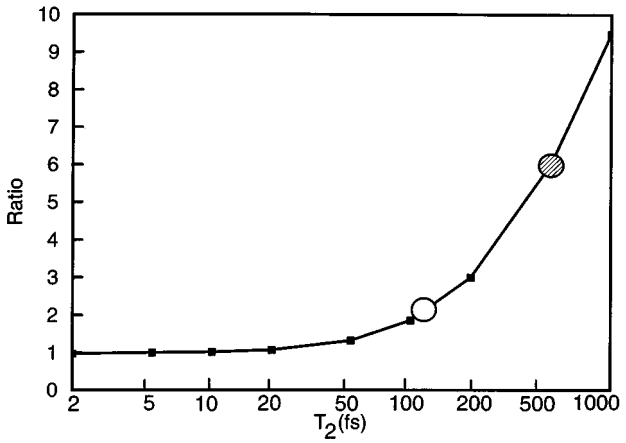


FIG. 8. Squares with line: calculated ratio of the maximum energy of the 2PFWM signal for 400 and 80 fs Gaussian pulses vs the phenomenological dephasing time $T_2$ for diphenyl acetylene (DPA) in a room temperature solvent. Open circle: Experimental ratio for DPA in room temperature 2-methyl pentane yielding a dephasing time $T_2=120$ fs. Hatched circle: Experimental ratio for DPA in room temperature cyclohexane yielding a dephasing time $T_2=500$ fs.

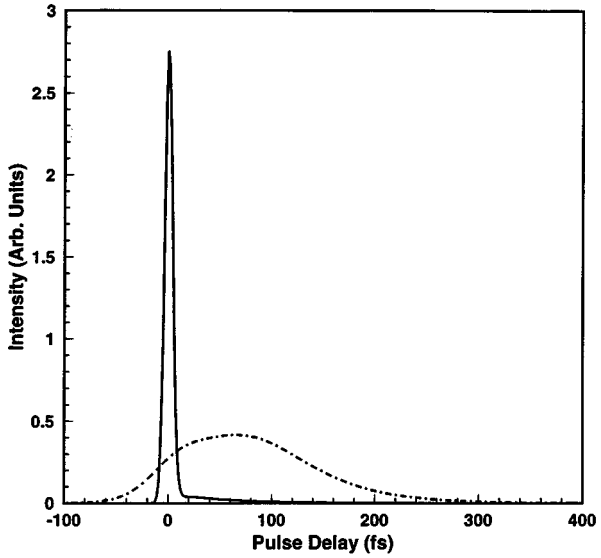


FIG. 9. Numerically calculated two pulse photon echo decays showing the integrated echo pulse intensity vs excitation pulse delay for a phenomenological $T_2=200$ fs (50 fs decay). The calculations include a nonresonant polarization component which responds instantly to the field in addition to the signal from the resonant two level system. The calculation method and other parameters are discussed in the text. Dashed line: pulse 1 and 2, 80 fs. The strength of $X_{\rm nr}^{(3)}$ has been adjusted so that the nonresonant component is 0.25 of resonant component, as found in the experiments. Solid line: pulse 1 and 2, 15 fs. The strength of $X_{\rm nr}^{(3)}$ and the pulse energy are the same as in the calculation for the 80 fs pulses. For 15 fs pulses, the large peak is the nonresonant signal. The tail is the resonant echo decay.

dressed using the calculation method of Appendix B, is whether shortening the pulse would make it possible to obtain traditional echo decay curves in spite of the competing nonresonant component. For the model calculation, the nonresonant component will be taken to be instantaneous, although the actual nonresonant component had some pulse duration dependence which was not modeled since only an experimental ratio was needed to analyze the data. For an instantaneous response, the intensity would go as the cube of the pulse's peak intensity, which would be greater for a shorter, but equal energy pulse. As the previous results show, the shorter pulse would result in a weaker resonant component. The two trends work against detection of an echo decay.

Figure 9 shows the numerically calculated combined resonant and nonresonant 2PFWM signal versus pulse delay for a phenomenological $T_2=200$ fs (50 fs echo decay). This value for $T_2$ was chosen to illustrate a decay which might barely be resolvable with deconvolution and excellent signal to noise with an 80 fs pulse but in principle should be be resolved easily with a 15 fs pulse. The calculations include the nonresonant polarization component which responds instantly to the field in addition to the signal from the resonant two level system. The strength of the nonresonant component used in the calculations corresponds to the one measured in the 2PFWM experiment on DPA in 2MP for an 80 fs pulse. The dashed line shows the result for 80 fs FWHM Gaussian pulses. The strength of $\chi_{\rm nr}^{(3)}$ has been adjusted so that the nonresonant component is 0.25 of resonant component. The solid line shows the results for 15 fs FWHM Gaussian pulses. The strength of $\chi_{\rm hr}^{(3)}$ and the pulse energy is the same as the calculation for the 80 fs pulses. By decreasing the pulse length by about a factor of 5, the resonant echo decay is now only $\sim$0.01 that of the nonresonant signal. While the 15 fs pulse can resolve the two pulse echo decay temporally, severe demands are placed on the experimental signal-to-noise ratio. The decay is a very small tail on the very large nonresonant signal. A pulse shape other than a Gaussian, which is wider in the wings, would make the situation worse by giving a broader base to the nonresonant component. Similar calculation were made assuming a much stronger nonresonant component, such as one might find in a highly polarizable liquid such as benzene. The results show that the problem is far worse. By decreasing the pulse length by about a factor of 5, the maximum of the resonant echo decay is only $\sim$0.0001 that of the nonresonant signal.

## VI. CONCLUDING REMARKS

Using the pulse duration echo method, it was possible to determine homogeneous dephasing times for diphenyl acetylene in 2-methyl pentane and cyclohexane. The dephasing times of $T_2=120$ fs for 2MP and $T_2=500$ fs for cyclohexane are consistent with the description of dephasing put forth by Walsh and Loring[9] for photon echoes on nonpolar chromophores in nonpolar fluids. Loring and Walsh's MD calculations suggested that the electronic dephasing in liquids arises primarily from the slight rearrangement of the first solvation shell about the chromophore. Since the viscosity of cyclohexane is 5 times greater than that of 2-methyl pentane, DPA in cyclohexane might be expected to exhibit a longer dephasing time. This is consistent with our data. The dephasing time in 2MP is relatively fast, but 2MP at room temperature is a very low viscosity liquid near its boiling point. The

$T_2$ of DPA in cyclohexane is substantially longer than that observed previously for a chromophore in a room temperature liquid. The difference in the viscosities is a low frequency property of the solvent. The question arises as to whether there is a direct correlation between the dephasing on the hundreds of fs time scale and the macroscopic viscosity for nonpolar systems.

When working in the UV, presence of substantial nonresonant signal from the solvent is a significant problem for the use of a two pulse echo. If the three pulse stimulated photon echo configuration is used, the signal will phase match in a unique direction, separate from the photon echo. If the stimulating pulse (the third pulse) is separated in time from the second pulse so that their intensity does not overlap, the instantaneous nonresonant signal will not scatter in the stimulated echo direction, even when the first two pulses overlap at $\tau=0$. The fact that the stimulating pulse has to be delayed for a number of pulse widths to prevent overlap and the generation of a nonresonant signal, means contributions that form spectral diffusion will contribute to the decay. For very short pulses, the separation between the second and third pulses would not have to be more than 100 fs, and the contribution from spectral diffusion might not be great.

The experimental technique that has been presented permits the extraction of $T_2$'s with pulses that are too long to actually observe the echo decay. However, the method requires the availability of at least two transform limited pulse durations. In the visible, where the nonresonant contribution is not substantial, the application of this method would be less difficult. The strong nonresonant signals that arise in UV 2PFWM experiments put severe restrictions on the ability to perform UV 2 pulse photon echo experiments where fast dephasing times are expected.

## ACKNOWLEDGMENT

This work was supported by the National Science Foundation, Division of Materials Research (DMR93-22504).

## APPENDIX A: EFFECT OF LINEAR ABSORPTION ON 2PFWM (INNER FILTER)

The pulse duration dependent 2PFWM data must be corrected for the linear absorbance (inner filter) of the solute as described in Sec. IV. The inner filter effect will be modeled using Beer's law rather than the complex frequency dependent linear susceptibility $\chi^{(1)}(\omega)$. The spectrum of the incident optical pulse is taken to be relatively narrow in comparison to the spectrum of the electronic absorbance. Beer's law is given for the electric field $E$ as

$$E=E_0\ \exp[-\tfrac{1}{2}\ln(10)\epsilon lc]=E_0\ \exp[-\tfrac{1}{2}\ln(10)A], \tag{A1}$$

where $E$ is the field transmitted through a sample length, $l$, with chromophore concentration $c$, and molar absorptivity $\epsilon$ given an initial intensity of $E_0$. The dimensionless absorbance $A$ is given by $A=\epsilon lc$.

The total third order nonlinear polarization from the differential area at a distance $l'$ into a sample of length $l$ due to the three attenuated input optical fields with maximum electric field $E_0$ is given by combining Eq. (4.1) with Eq. (A1):

$$P^{(3)}_{\rm tot}(l')dl'=\hat{\chi}^{(3)}_{\rm tot}[E_0\ \exp(-\tfrac{1}{2}\ln 10\epsilon c l')]^3 dl'. \tag{A2}$$

The signal field generated by this polarization must propagate through the remainder of the sample as well and thus will also be attenuated. The signal field is proportional to the polarization; the signal field from location $l'$ as attenuated at the end of the sample $l$ is given by

$$\begin{aligned}E_s(l)&=\int_0^l P^{(3)}_{\rm tot}(l')\ \exp[-\tfrac{1}{2}\ln 10\epsilon c(l-l')]dl'\\&=\int_0^l \hat{\chi}^{(3)}_{\rm tot}[E_0\ \exp(-l')]^3\\&\quad\times\exp[-\tfrac{1}{2}\ln 10\epsilon c(l-l')]dl'.\end{aligned} \tag{A3}$$

The intensity is related to the electric field by $I\propto|E|^2$. In practice, it is easiest to vary the energy, or time integrated intensity of the pulse. The energy of the pulse will be denoted as $U$. For simplicity, the pulses are taken to be square, which does not change the nature of the results:

$$U_0=\int E_0^2 dt\approx E_0^2\tau_p. \tag{A4}$$

Again, $\tau_p$ is the length of the pulse. The pulse duration $\tau_p$ has only been introduced here to properly normalize the amplitude of the electric fields. It is shown in Eq. (4.4), which describes an observable for this experiment, that the quantities $\tau_p$ cancel. Equivalently the electric field of a pulse with a given width and energy is

$$E_0=\left(\frac{U_0}{\tau_p}\right)^{1/2}. \tag{A5}$$

The signal pulse will be as long as the input pulse so long as the inverse total line width is shorter than the pulse duration $\tau_p$. The measured energy will then be

$$U_{\rm tot}=\int I_{\rm tot}dt=\beta_{\rm tot}I_{\rm tot}\tau_p. \tag{A6}$$

The factor $\beta_{\rm tot}$ corrects for the slight change in pulse shape of the signal.

With the assumption that the dispersive properties of the susceptability are minimal, then for the polarization given by Eq. (4.1), the complex quantities may be replaced by their modulus, i.e.,

$$P^{(3)}_{\rm tot}(\omega)=|\hat{\chi}^{(3)}_{\rm tot}(\omega)E_1^*E_2^2|=|\hat{\chi}^{(3)}_{\rm tot}(\omega)||E|^3. \tag{A7}$$

Using the relationship for the absorbance $A$, Eq. (4.7) can be evaluated in terms of the observable energy to give the expression for the two pulse four wave mixing or photon echo signal as attenuated by the ''inner filter'' effect:

$$U_{\rm tot}\propto\beta_{\rm tot}|\hat{\chi}^{(3)}_{\rm tot}|^2\ \frac{U_0^3}{\tau_p^2}\ l^2\ \frac{10^{-A}[10^{-A}-1]^2}{(\ln 10)^2A^2}. \tag{A8}$$

In practice, one wishes to compare the intensity of the nonresonant signal generated by the solvent alone with the

total signal generated by the solvent and chromophore. The pure solvent has no absorbance and therefore no inner filter. The expression for the nonresonant signal from the pure solvent is

$$U_{\mathrm{nr}} \propto \beta_{\mathrm{nr}} |\hat{\chi}_{\mathrm{nr}}^{(3)}|^2 \frac{U_0^3}{\tau_p^2} I^2. \tag{A9}$$

The inner filter factor is given by the right most term of Eq. (A8). Explicitly, the inner filter function for the third order polarization is

$$f^{(3)}(A) = \frac{10^{-A}[10^{-A}-1]^2}{(\ln 10)^2 A^2}. \tag{A10}$$

This third order inner filter function $f^{(3)}(A)$ is plotted versus absorbance $A$ in Fig. 3. Experiments are commonly performed on samples with absorbances between 0 and 1. When there is no absorbance, $f^{(3)}(A=0)=1$. An absorbance $A=1$ indicates 90% linear attenuation of the intensity. This absorbance corresponds to $f^{(3)}(A=1)\approx 0.015$. Given a maximum inner filter factor of 0.015, as long as the ratio of the susceptibilities $|\hat{\chi}_{\mathrm{tot}}^{(3)}|^2/|\hat{\chi}_{\mathrm{nr}}^{(3)}|^2$ is greater than 67, the observed ratio $U_{\mathrm{tot}}/U_{\mathrm{nr}}$ will be greater than 1 for any absorbance between 0 and 1. This corresponds to the situation where experiments are performed in the visible with a laser dye as a chromophore. If however the ratio of the susceptibilities is less than 67, the observed ratio $U_{\mathrm{tot}}/U_{\mathrm{nr}}$ will be less than 1 for any absorbance between 0 and 1. This corresponds to the UV experiments described here where the nonresonant susceptibility of the solvent is strong and the transition dipole moment of the chromophore is weaker than in visible wavelength systems studied previously.

## APPENDIX B: EFFICIENT NUMERICAL SIMULATION OF 2PFWM

As discussed in Sec. IV, unless unphysical delta function pulses are assumed, the evaluation of the 2PFWM (photon echo) signal energy $U_s(\tau,\xi(t;\tau_p),T_2)$ in Eq. (4.14) must be done numerically. Calculation of the signal of a pulse duration ($\tau_p$) dependent 2PFWM experiment must use realistic, finite duration pulse envelopes $\xi(t,\tau_p)$. Even if the pulse separation is restricted to one time $\tau$, determining the homogeneous dephasing time $T_2$ by Eq. (4.15) requires calculating the 2PFWM signal $U_s(\xi(t;\tau_p),T_2)$ and, therefore, the numerical evaluation of a complex, five dimensional integral for two values of $\tau_p$, and many values of $T_2$.

The evaluation of true five dimensional integrals using simple interval sampling numerical methods (trapezoid rules, Gaussian integration) is in general not practical even with the fastest computers. Wiersma *et al.* used a Monte Carlo method of integration[30] to evaluate chirped four wave mixing and multimode Brownian oscillator expressions. This method seemed unsuitable for absolute numerical work, since there is no assurance of rapid convergence.

However, the standard trapezoidal interval sampling method may be implemented in a way that reuses the previous evaluations of the inner integrals in the time ordered perturbation expression for the polarization $P^{(3)}$. If the functional form of the Liouville Green function propagators is restricted to an exponential with truncated Taylor series arguments, it is possible to reduce the order of the algorithm so that the calculation may be performed in a reasonable period of time as outlined below. This routine is efficient enough that the 2PFWM (photon echo) signal may be rapidly calculated as a function of pulse separation $\tau$, yielding the photon echo decay (see Fig. 9) as well as its application to fitting $T_2$ using Eq. (4.15).

The complexity of the evaluation of the integral in Eq. (4.11) can be seen to be wholly dependent on the complexity of the evaluation of $P^{(3)}$. The numerical integration of the inhomogeneous distribution of chromophore transition energies, $\omega_{\mathrm{ba}}$, was performed in the frequency domain. The final time integration of the intensity at $t_s$ is not very difficult and is made easier by the fact that the modulus square of the polarization $P^{(3)}$ is a slowly varying envelope. Thus the portion of the expression which benefits the most from simplification and/or efficient evaluation of integrals is the third order nonlinear polarization $P^{(3)}$.

As an example, the expression for one of the photon echolike rephasing terms of is given:

$$\begin{aligned} P_{\mathrm{I}}^{(3)}[ts;\xi(\tau_p)] = \left(\frac{1}{1\hbar}\right)^3 & \rho_{\mathrm{aa}}^{(0)} \mu_{\mathrm{ab}}^{\mathbf{k}_2} \mu_{\mathrm{ba}}^{\mathbf{k}_s} \mu_{\mathrm{ab}}^{\mathbf{k}_2} \mu_{\mathrm{ab}}^{\mathbf{k}_1} E_{\mathbf{k}_1}^{*} E_{\mathbf{k}_2}^{2} \exp(i\mathbf{k}_s\mathbf{r}) \\ & \times \int_{-\infty}^{t_s} dt_3 \int_{-\infty}^{t_3} dt_2 \int_{-\infty}^{t_2} dt_1 G_{\mathrm{ab}}(t_2-t_1) \\ & \times G_{\mathrm{bb}}(t_3-t_2) G_{\mathrm{ba}}(t_s-t_3) \\ & \times [\xi_{\mathbf{k}_1}(t_1)\ \exp(i\omega_a t_1)] \\ & \times [\xi_{\mathbf{k}_2}(t_2-\tau)\ \exp(-i\omega_a(t_2-\tau))] \\ & \times [\xi_{\mathbf{k}_2}(t_3-\tau)\ \exp(-i\omega_a(t_3-\tau))]. \end{aligned} \tag{B1}$$

$\rho_{ii}^{(0)}$ is the initial density matrix element for this quantum pathway $I$, $\mu_{ij}^{\mathbf{k}_1}$ is the transition dipole moment between states $i$ and $j$ along wave vector $\mathbf{k}_1$, $E_{\mathbf{k}_1}$ is a complex coefficient describing the maximum electric field of the plane wave along wave vector $\mathbf{k}_1$, $\exp(i\mathbf{k}_s\mathbf{r})$ describes the spatial characteristics of the generated polarization, $G_{ij}(t''-t')$ is the Liouville propagator that describes the evolution of the density matrix element $\rho_{ij}$ between times $t''$ and $t'$, $\xi_{\mathbf{k}_1}(t')$ is the slowly varying envelope that the describes the temporal shape of the plane wave with wave vector $\mathbf{k}_1$, and $\exp(i\omega_a t')$ is the appropriate Fourier component of the electromagnetic field along the same wave vector. $\xi(\tau_p)$ denotes that the expression will be dependent on the realistic pulse envelope and the pulse duration, $\tau_p$.

The complex nature of the integration necessary to evaluate $P^{(3)}$ in Eq. (B1) can be seen to stem from two main sources: (1) The upper limit of integration of an inner integrand becomes a variable of integration for the next outer integrand, and (2) the expression for each propagator $G_{ij}(t''-t')$ may not be linearly separable in $t''$ and $t'$. Note however that each envelope and plane wave expression $\xi_{\mathbf{k}_1}(t')\exp[i\omega_a t']$ contains only one variable of integration.

Equation (B1) can be factored somewhat to give the following form:

$$P_{\mathrm{I}}^{(3)}(t_s) = \left(\frac{1}{i\hbar}\right)^3 \rho_{\mathrm{aa}}^{(0)} \mu_{\mathrm{ab}}^{\mathbf{k}_2} \mu_{\mathrm{ba}}^{\mathbf{k}_s} \mu_{\mathrm{ab}}^{\mathbf{k}_2} \mu_{\mathrm{ba}}^{\mathbf{k}_1} E_{\mathbf{k}_1}^{*} E_{\mathbf{k}_2}^{2} \exp(i\mathbf{k}_s\mathbf{r}) \times \int_{-\infty}^{t_s} dt_3 G_{\mathrm{ba}}(t_s - t_3)[\xi_{\mathbf{k}_2}(t_3-\tau) \exp(-i\omega_a(t_3-\tau))] \times \int_{-\infty}^{t_3} dt_2 G_{\mathrm{bb}}(t_3 - t_2)[\xi_{\mathbf{k}_2}(t_2-\tau) \exp(-i\omega_a(t_2-\tau))] \times \int_{-\infty}^{t_2} dt_1 G_{\mathrm{ab}}(t_2 - t_1)[\xi_{\mathbf{k}_1}(t_1) \exp(i\omega_a t_1)]. \quad \text{(B2)}$$

The propagator chosen for the actual numerical calculations is of the form:

$$G_{ij}(t''-t') = \exp[-\Omega_{ij}(t''-t')]. \quad \text{(B3)}$$

The phenomenological damping function $\Omega_{ij}(t''-t')$ is the simplest realistic damping function for any two elements of the density matrix and is given by the linear equation

$$\Omega_{ij}(t') = \Omega_{ij} t', \quad \text{(B4)}$$

where $\Omega_{ij}$ is now only a complex number and not a function. $\Omega_{ij}$ is defined as

$$\Omega_{ij} = \omega_{ij} - i\Gamma_{ij}, \quad \text{(B5)}$$

where $\omega_{ij}$ is the angular Bohr transition frequency between states $i$ and $j$,

$$\omega_{ij} = \frac{E_i - E_j}{\hbar}. \quad \text{(B6)}$$

$\Gamma_{ij}$ is the total dephasing rate between states $i$ and $j$ given by

$$\Gamma_{ij} = \gamma_i + \gamma_j + \gamma_{ij}, \quad \text{(B7)}$$

where $\gamma_i$ and $\gamma_j$ population decay rates out of states $i$ and $j$, and $\gamma_{ij}$ is the pure dephasing rate between states $i$ and $j$.

Note that this phenomenological damping function is only an approximation to the solution for the equation of motion of the density matrix. The damping function does not conserve population. The population decay rates should be considered to be delivering population to a long lived ''dark'' state that is not otherwise involved in the calculation. Since the experimental dephasing times are much shorter than the lifetime, this approximation is of no consequence. For the calculations described below, $\gamma_{ij} \gg \gamma_i + \gamma_j$ so that $\Gamma_{ij} \cong \gamma_{ij}$. This is consistent with the measured value of $T_1$. Calculations for a particular homogeneous dephasing time $T_2$ have been made by setting $\Gamma_{ij} = 1/T_2$, where the definition of the dephasing time $T_2$ is the same as in the Bloch picture.

Using the definition of the damping Green function, the expressions for the polarization may be factored further. The factored expressions for all four diagrams are:

$$P_{\mathrm{I}}^{(3)}(t_s) = \left(\frac{1}{i\hbar}\right)^3 \rho_{\mathrm{aa}}^{(0)} \mu_{\mathrm{ab}}^{\mathbf{k}_2} \mu_{\mathrm{ba}}^{\mathbf{k}_s} \mu_{\mathrm{ab}}^{\mathbf{k}_2} \mu_{\mathrm{ba}}^{\mathbf{k}_1} E_{\mathbf{k}_1}^{*} E_{\mathbf{k}_2}^{2} \exp(i\mathbf{k}_s\mathbf{r}) \times \exp(-i(\Omega_{\mathrm{ba}} t_s - 2\omega_a\tau)) \times \int_{-\infty}^{t_s} dt_3 \xi_{\mathbf{k}_2}(t_3-\tau) \exp(-i[-\Omega_{\mathrm{ba}} + \Omega_{\mathrm{bb}} + \omega_a]t_3) \times \int_{-\infty}^{t_3} dt_2 \xi_{\mathbf{k}_2}(t_2-\tau) \exp(-i[-\Omega_{\mathrm{bb}} + \Omega_{\mathrm{ab}} + \omega_a]t_2) \times \int_{-\infty}^{t_2} dt_1 \xi_{\mathbf{k}_1}(t_1) \exp(-i[-\Omega_{\mathrm{ab}} - \omega_a]t_1), \quad \text{(B8)}$$

$$P_{\mathrm{II}}^{(3)}(t_s) = \left(\frac{1}{i\hbar}\right)^3 \rho_{\mathrm{aa}}^{(0)} \mu_{\mathrm{ab}}^{\mathbf{k}_2} \mu_{\mathrm{ba}}^{\mathbf{k}_s} \mu_{\mathrm{ab}}^{\mathbf{k}_2} \mu_{\mathrm{ba}}^{\mathbf{k}_1} E_{\mathbf{k}_1}^{*} E_{\mathbf{k}_2}^{2} \exp(i\mathbf{k}_s\mathbf{r}) \times \exp(-i(\Omega_{\mathrm{ba}} t_s - 2\omega_a\tau)) \times \int_{-\infty}^{t_s} dt_3 \xi_{\mathbf{k}_2}(t_3-\tau) \exp(-i[-\Omega_{\mathrm{ba}} + \Omega_{\mathrm{aa}} + \omega_a]t_3) \times \int_{-\infty}^{t_3} dt_2 \xi_{\mathbf{k}_2}(t_2-\tau) \exp(-i[-\Omega_{\mathrm{aa}} + \Omega_{\mathrm{ab}} + \omega_a]t_2) \times \int_{-\infty}^{t_2} dt_1 \xi_{\mathbf{k}_1}(t_1) \exp(-i[-\Omega_{\mathrm{ab}} - \omega_a]t_1), \quad \text{(B9)}$$

$$P_{\mathrm{III}}^{(3)}(t_s) = \left(\frac{1}{i\hbar}\right)^3 \rho_{\mathrm{aa}}^{(0)} \mu_{\mathrm{ab}}^{\mathbf{k}_2} \mu_{\mathrm{ba}}^{\mathbf{k}_s} \mu_{\mathrm{ab}}^{\mathbf{k}_2} \mu_{\mathrm{ba}}^{\mathbf{k}_1} E_{\mathbf{k}_1}^{*} E^2{}_{\mathbf{k}_2} \times \exp(ik_s\mathbf{r}) \exp(-i(\Omega_{\mathrm{ba}} t_s - 2\omega_a\tau)) \times \int_{-\infty}^{t_s} dt_3 \xi_{\mathbf{k}_2}(t_3-\tau) \exp(-i[-\Omega_{\mathrm{ba}} + \Omega_{\mathrm{bb}} + \omega_a]t_3) \times \int_{-\infty}^{t_3} dt_2 \xi_{\mathbf{k}_1}(t_2) \exp(-i[-\Omega_{\mathrm{bb}} + \Omega_{\mathrm{ba}} - \omega_a]t_2) \times \int_{-\infty}^{t_2} dt_1 \xi_{\mathbf{k}_2}(t_1-\tau) \exp(-i[-\Omega_{\mathrm{ba}} + \omega_a]t_1), \quad \text{(B10)}$$

$$P_{\mathrm{IV}}^{(3)}(t_s) = \left(\frac{1}{i\hbar}\right)^3 \rho_{\mathrm{aa}}^{(0)} \mu_{\mathrm{ab}}^{\mathbf{k}_2} \mu_{\mathrm{ba}}^{\mathbf{k}_s} \mu_{\mathrm{ab}}^{\mathbf{k}_2} \mu_{\mathrm{ba}}^{\mathbf{k}_1} E_{\mathbf{k}_1}^{*} E^2{}_{\mathbf{k}_2} \times \exp(i\mathbf{k}_s\mathbf{r}) \exp(-i(\Omega_{\mathrm{ba}} t_s - 2\omega_a\tau)) \times \int_{-\infty}^{t_s} dt_3 \xi_{\mathbf{k}_2}(t_3-\tau) \exp(-i[-\Omega_{\mathrm{ba}} + \Omega_{\mathrm{aa}} + \omega_a]t_3) \times \int_{-\infty}^{t_3} dt_2 \xi_{\mathbf{k}_1}(t_2) \exp(-i[-\Omega_{\mathrm{aa}} + \Omega_{\mathrm{ba}} - \omega_a]t_2) \times \int_{-\infty}^{t_2} dt_1 \xi_{\mathbf{k}_2}(t_1-\tau) \exp(-i[-\Omega_{\mathrm{ba}} + \omega_a]t_1). \quad \text{(B11)}$$

These factored expressions can be evaluated using a modified trapezoid rule relatively efficiently. If the necessary grid density and limits of each integral are similar (as they are in these factored expressions of $P^{(3)}$), the two integrals may be made to share the same limits and evaluation grid. If they share the same grid, the value of the inner integral at each point (from the lower limit to the upper limit and each point in between) can be stored in an array indexed by the common grid. Thus the computational expense becomes linear, rather than cubic, in the number of points necessary to evaluate the oscillatory integrands over the length of the pulse. The evaluation of the third order nonlinear polarization has been reduced to essentially a one dimensional integral. Considering the integrations over the inhomogeneous line and the time dependent intensity, this means that only an effective three dimensional integral need be evaluated in order to compute the photon echo/2PFWM. In this method, the computation time and memory scale linearly in the pulse length, and therefore it is not appropriate for pulses tens of picoseconds long.

This algorithm was implemented in the *C* programming language, and the numerical evaluation was performed using up to 10 IBM model 3BT and 375/6000 workstations. The curves shown in Fig. 9 took about 2 h of calculation time to generate.


[1] P. C. Becker, H. L. Fragnito, J. Y. Bigot, C. H. B. Cruz, R. L. Fork, and C. V. Shank, Phys. Rev. Lett. **63**, 505 (1989).
[2] E. T. J. Nibbering, D. A. Wiersma, and K. Duppen, Phys. Rev. Lett. **66**, 2464 (1991).
[3] W. P. d. Boeji, M. S. Pshenichnikov, and D. A. Wiersma, Chem. Phys. Lett. **238**, 1 (1995).
[4] P. Vohringer, D. C. Arnett, T. S. Yang, and N. F. Scherer, Chem. Phys. Lett. **237**, 387 (1995).
[5] J. Y. Bigot, M. T. Portella, R. W. Shoenlein, C. J. Bardeen, A. Migus, and C. V. Shank, Phys. Rev. Lett. **66**, 1138 (1989).
[6] T. Joo and A. C. Albrecht, Chem. Phys. **176**, 233 (1993).
[7] C. H. B. Cruz, R. L. Fork, W. H. Knox, and C. V. Shank, Chem. Phys. Lett. **132**, 341 (1986).
[8] W. P. d. Boeij, M. S. Pshenichnikov, K. Duppen, and D. A. Wiersma, Chem. Phys. Lett. **224**, 243 (1994).
[9] A. M. Walsh and R. F. Loring, Chem. Phys. Lett. **186**, 77 (1991).
[10] S. A. Adelman, Adv. Chem. Phys. **44**, 143 (1980).
[11] Y. J. Yan and S. Mukamel, Phys. Rev. A **41**, 6485 (1989).
[12] V. J. Newell, F. W. Deeg, S. R. Greenfield, and M. D. Fayer, J. Opt. Soc. Am. B **6**, 257 (1988).
[13] F. Gires and P. Tournois, C. R. Acad. Sci. Paris **258**, 6112 (1964).
[14] J. A. Giordmaine, M. A. Duguay, and J. W. Hansen, J. Quant. Electron. **QE-4**, 252 (1968).
[15] W. Rudolph and B. Wilhelmi, *Light Pulse Compression* (Harward Academic, Chur, 1989).
[16] J. G. Fujimoto, A. M. Weiner, and E. P. Ippen, Appl. Phys. Lett. **40**, 832 (1984).
[17] J. M. Halbout and D. Grischkowsky, Appl. Phys. Lett. **45**, 1281 (1984).
[18] W. H. Knox, R. L. Fork, M. C. Downer, R. H. Stolen, C. V. Shank, and J. Valdmanis, Appl. Phys. Lett. **46**, 1120 (1985).
[19] C. V. Shank, R. L. Fork, R. Yen, R. H. Stolen, and W. J. Tomlinson, Appl. Phys. Lett. **40**, 761 (1982).
[20] L. F. Mollenauer, R. H. Stolen, and J. P. Gordon, Phys. Rev. Lett. **45**, 1095 (1980).
[21] J. D. Kafka and T. Baer, Opt. Lett. **12**, 401 (1987).
[22] J. Herrmann and B. Wilhelmi, *Lasers For Ultrashort Light Pulses* (North-Holland, Amsterdam, 1987).
[23] D. Zimdars, Thesis, Standford University, 1996.
[24] R. Trebino and D. J. Kane, J. Opt. Soc. Am. A **10**, 1101 (1993).
[25] D. J. Kane and R. Trebino, J. Quant. Electron. **29**, 571 (1993).
[26] Y. Hirata, T. Okada, N. Mataga, and T. Nomoto, J. Phys. Chem. **96**, 6559 (1992).
[27] Y. R. Shen, *Principles of Nonlinear Optics* (Wiley, New York, 1984).
[28] R. F. Loring and S. Mukamel, Chem. Phys. Lett. **114**, 426 (1985).
[29] Y. J. Yan and S. Mukamel, J. Chem. Phys. **94**, 179 (1991).
[30] K. Duppen, F. d. Haan, E. T. J. Nibbering, and D. A. Wiersma, Phys. Rev. A **47**, 5120 (1993).
[31] M. D. Levenson and S. S. Kano, *Introduction to Nonlinear Laser Spectroscopy* (Academic, Boston, 1988).